Journal of Quantitative Spectroscopy & Radiative Transfer 233 (2019) 110–118

Contents lists available at ScienceDirect

Journal of Quantitative Spectroscopy & Radiative Transfer

journal homepage: www.elsevier.com/locate/jqsrt

Spectroscopic investigations of transition properties for the electronic states of PN^+ correlating to two lowest dissociation limits

Z. Qin[a], J.M. Zhao[a], L.H. Liu[a,b,*]

[a] School of Energy Science and Engineering, Harbin Institute of Technology, Harbin 150001, China
[b] School of Energy and Power Engineering, Shandong University, Qingdao 266237, China

ARTICLE INFO

Article history:
Received 19 April 2019
Revised 21 May 2019
Accepted 22 May 2019
Available online 23 May 2019

Keywords:
Transition probabilities
Ab initio calculations
Spectroscopic parameters
Spin-orbit couplings
PN^+

ABSTRACT

The PN^+ cation is regarded as a candidate of ions which may exist in the interstellar medium. Accurate transition properties are desired to identify the spectra from astronomical observation. However, transition data of PN^+ are relatively limited. In this work, the state-of-the-art *ab initio* calculations are carried out to investigate the low-lying electronic states of PN^+ correlating to two lowest dissociation limits, its transition properties and its spin-orbit couplings. For the $X^2\Sigma^+$ and $A^2\Pi$ states, the calculated spectroscopic constants agree well with previous experimental data. For the other electronic states, the accuracy of the spectroscopic parameters is also ensured by comparing with previous theoretical results. Then, transition probabilities of dipole allowed transition systems are calculated. The radiative lifetimes of vibrational levels for the $A^2\Pi$, $1^4\Pi$, $1^4\Delta$, $1^4\Sigma^-$, and $2^4\Pi$ states are also evaluated. Such transition data can be used in the identification of PN^+ in the laboratory or the interstellar space. Finally, the predissociation of $1^4\Sigma^-$ ($\upsilon' = 1$)→$1^6\Sigma^+$, $1^4\Sigma^-$ ($\upsilon' = 15$)→$1^6\Pi$ and $1^4\Delta$ ($\upsilon' = 19$)→$1^6\Pi$ are analyzed with the help of spin-orbit coupling integrals.

1. Introduction

Development of spectroscopy has stimulated the interest of more and more researchers in studying various diatomic molecular systems in the gas phase. Phosphorus mononitride (PN) is an astrophysically important molecule that has been detected in different regions of the interstellar medium (ISM) [1–11]. As of yet there are no observations of its cation PN^+ in the interstellar space. A number of experimental and theoretical work has been done to investigate the spectral transitions of PN molecule [12–32]. However, available spectral transitions of PN^+ are extremely limited. For example, vibrational transitions in the 305–393 nm region were observed by Obase et al. [33–35] for the $B^2\Sigma^+ - X^2\Sigma^+$ system, including band-head wavelengths and relative band intensities. The Morse Franck-Condon factors and r-centroids of the $B^2\Sigma^+ - X^2\Sigma^+$ system were approximately calculated. Furthermore, the variation of the electric transition moment against r-centroid $r_{\upsilon'\upsilon''}$ is presented for $1.439 \le r_{\upsilon'\upsilon''} \le 1.647$ Å. But these few transition data are based on some approximate treatments. A more up-to-date rotational transition frequencies of the $B^2\Sigma^+(\upsilon = 0)$–$X^2\Sigma^+(\upsilon = 0)$ transition were given by Imajo et al. [36]. No other transition data of PN^+ are given in the literature.

There have been several studies aimed to obtain the potential energy curves (PECs) and spectroscopic parameters of PN^+ from theoretical calculations and experimental observations [33–42]. A review of the experimental work on PN^+ till 2000 was given by Imajo et al. [36]. Three states ($X^2\Sigma^+$, $A^2\Pi$, and $B^2\Sigma^+$) have been observed in the experiments. Theoretically, only Gein [38] and Zhu et al. [42] studied the PECs and spectroscopic constants for low-lying excited states of PN^+, including quartet and sextet Λ-S states and their corresponding Ω states. However, there have not been theoretical investigations of transition properties for PN^+ in the literature.

It has been pointed out that PN^+, N_2^+, and P_2^+ have some similar characteristics since they all have nine valence electrons [36,38]. Both theoretical and experimental studies proposed the existence of couplings between close lying electronic states of N_2^+ and P_2^+ via spin-orbit (SO) interactions [41,43–45]. However, there are no theoretical treatments of SO interactions for PN^+.

The aim of this work is to calculate dipole allowed transitions of PN^+ and to investigate the interactions between different electronic states of PN^+ with the SO coupling integrals. To this end, the state-of-the-art ab initio method is used to calculate the PECs and transition dipole moments (TDMs) of PN^+, which are then employed to compute dipole allowed transition probabilities. The

* Corresponding author.
E-mail address: liulinhua@sdu.edu.cn (L.H. Liu).

https://doi.org/10.1016/j.jqsrt.2019.05.024
0022-4073/

Table 1
Dissociation correlations of nine electronic states of PN^+ resulting from the first and second dissociation limits.

Dissociation limit	Electronic state	Relative energy (cm^{-1})	
		This work[a]	Exp. [46]
$P^+(^3P_g)+N(^4S_u)$	$X^2\Sigma^+$, $A^2\Pi$, $1^4\Sigma^+$, $1^4\Pi$, $1^6\Sigma^+$, $1^6\Pi$,	0.00	0.00
$P^+(^1D_g)+N(^4S_u)$	$1^4\Sigma^-$, $2^4\Pi$, $1^4\Delta$	8356.86	8882.31

[a] Obtained by the icMRCI + Q/56 + CV + DK calculations.

highly correlated wave functions are also obtained, which are used to evaluate the SO coupling integrals between low-lying electronic states of PN^+.

2. Computational approaches

2.1. Dissociation correlations

The ionization energies of P and N atoms are 84,580.83 ± 0.12 and 117,225.7 ± 0.3 cm^{-1} [46], respectively. Hence, a P atom is easier to dissociate than a N atom. That is to say, the first dissociation limit of PN^+ is $P^+(^3P_g)$ + $N(^4S_u)$. Note that the $(3p^2)$ ^3P_g and $(2p^3)$ ^4S_u are the ground states of P^+ and N. The first excited states of P^+ and N are $(3p^2)^1D_g$ and $(2p^3)^2D_u$, which are 19,228.82 and 8882.31 cm^{-1} relative to their respective ground states [46], so the second dissociation limit of PN^+ is $P^+(^1D_g)$ + $N(^4S_u)$. Table 1 presents the dissociation correlations of nine electronic states resulting from the first two dissociation limits, together with the energy separation between the first and second dissociation limits, which agrees well with the experimental value [46].

2.2. Transition properties

The complete active space self-consistent field (CASSCF) method [47] in conjunction with the subsequent internally contracted multi-reference configuration interaction (icMRCI) approach [48,49] with the Davidson correction (+Q) is used for the calculations of PECs of PN^+ with the aug-cc-pV6Z basis set, for the core-valance (CV) correction calculations with the cc-pCV5Z [50] basis set, and for the scalar relativistic correction calculations with the cc-pV5Z-DK basis set [51]. The aug-cc-pV5Z (AV5Z) and aug-cc-pV6Z (AV6Z) basis sets are adopted to extrapolate the potential energy to the CBS limit. The basis extrapolation formulas are given by [52,53]

$$E_X^{ref} = E_\infty^{ref} + A^{ref}X^{-\alpha} \tag{1}$$

$$E_X^{cor} = E_\infty^{cor} + A^{cor}X^{-\beta} \tag{2}$$

where, E_X^{ref} and E_X^{cor} are, respectively, the reference energy (denoted by the superscript "*ref*") and the correlation energy (denoted by the superscript "*cor*") calculated with the aug-cc-pVXZ ($X = 5$ or 6) basis set. E_∞^{ref} and E_∞^{cor} are the CBS extrapolation energies, the subscript "∞" refers to the CBS limit. α and β are the extrapolation parameters ($\alpha = 3.4$, $\beta = 2.4$). TDMs are computed by the icMRCI method with the AV6Z basis set. These calculations are performed in the MOLPRO 2015 program suite [54,55].

In the calculations, 12 inner electrons are put into six closed-shell molecular orbitals (MOs) in the symmetry representations of C_{2v}: four a_1 orbitals, one b_1 orbital, one b_2 orbital, and no a_2 orbitals. The remaining 9 electrons are put into 9 outermost MOs, which constitute the active space: five a_1 orbitals, two b_1 orbital, two b_2 orbital, and no a_2 orbitals. The orbital set is called (9,3,3,0).

To our knowledge, optical diagnostics, astronomical observation and radiation modeling require accurate transition probabilities [56]. Using the obtained PECs and TDMs, we can determine the transition probabilities of a certain electronic transition system. The key parameter of calculating transition probabilities is the square of the electronic-vibrational transition moment $\left(R_e^{\upsilon'\upsilon''}\right)^2$

$$\left(R_e^{\upsilon'\upsilon''}\right)^2 = \left[\int_0^\infty \psi_{\upsilon'}(r)R_e(r)\psi_{\upsilon''}(r)dr\right]^2 \tag{3}$$

where υ' and υ" are the vibrational levels of upper and lower electronic states, respectively, $\psi_{\upsilon'}$ and $\psi_{\upsilon''}$ are the corresponding vibrational wave functions, r is the internuclear distance, and $R_e(r)$ is the TDM function. Once the square of the electronic-vibrational transition moment is obtained, Einstein coefficients of spontaneous emissions (hereafter called Einstein coefficients) $A_{\upsilon'\upsilon''}$ can be calculated by [56,57]

$$A_{\upsilon'\upsilon''} = 2.026\times10^{-6}\sigma_{\upsilon'\upsilon''}^3\frac{2-\delta_{0,\Lambda'+\Lambda''}}{2-\delta_{0,\Lambda'}}\left(R_e^{\upsilon'\upsilon''}\right)^2 \tag{4}$$

where $\sigma_{\upsilon'\upsilon''}$ is the wavenumber of the transition system, Λ' and Λ" are the projections of electronic orbital angular momentums on the internuclear axis for upper and lower electronic levels, respectively. Another important transition probability is the Franck-Condon factor $q_{\upsilon'\upsilon''}$, which can be computed by [56,57]

$$q_{\upsilon'\upsilon''} = \left(\int \psi_{\upsilon'}(r)\psi_{\upsilon''}(r)dr\right)^2 \tag{5}$$

Based on the Einstein coefficients, the radiative lifetime $\tau_{\upsilon'}$ of a certain vibrational level υ' for the upper electronic state can be determined by

$$\tau_{\upsilon'} = \frac{1}{\sum_{\upsilon''=0}^{\upsilon''_{\max}} A_{\upsilon'\upsilon''}} \tag{6}$$

2.3. Spin-orbit couplings

In general, the whole Hamiltonian of a given molecular system is made up of the spin-free Hamiltonian $\hat{H}^{SF}$ and the SO part of Breit-Pauli Hamiltonian $\hat{H}^{SO}$

$$\hat{H} = \hat{H}^{SF} + \hat{H}^{SO} \tag{7}$$

The Breit-Pauli SO operator $\hat{H}^{SO}$ can be expressed as [58],

$$\hat{H}^{SO} = \sum_\alpha\left[\sum_i \hat{h}_\alpha(i)\cdot\hat{s}_\alpha(i) + \sum_{i\neq j}\hat{g}_\alpha(i,j)\cdot\hat{s}_\alpha(i)\right] \tag{8}$$

where the first and second terms are known as the one-electron and two-electron operators, respectively. The one-electron $\hat{h}_\alpha(i)$ and two-electron $\hat{g}_\alpha(i,j)$ SO operators are defined as [58]

$$\hat{h}_\alpha(i) = \frac{1}{2c^2}\sum_K\frac{Z_K\left[\mathbf{r}_{iK}\times\hat{\mathbf{p}}(i)\right]_\alpha}{r_{iK}^3} \tag{9}$$

$$\hat{g}_\alpha(i,j) = -\left[2\hat{g}_{o\alpha}(i,j) + \hat{g}_{s\alpha}(i,j)\right] \tag{10}$$

with

$$\hat{g}_{o\alpha}(i,j) = \frac{1}{2c^2}\frac{\left[\mathbf{r}_{ij}\times\hat{\mathbf{p}}(j)\right]_\alpha}{r_{ij}^3} \tag{11}$$

Table 2
Main electron configurations of eight electronic states for PN^+ near their corresponding equilibrium internuclear distances.

State	Main electron configuration [a]	State	Main electron configuration [a]	State	Main electron configuration [a]
$X^2\Sigma^+$	$5\sigma^2 6\sigma^2 2\pi^4 7\sigma^1 3\pi^0$ (0.905)	$1^4\Delta$	$5\sigma^2 6\sigma^2 2\pi^3 7\sigma^1 3\pi^1$ (0.649)	$1^4\Sigma^-$	$5\sigma^2 6\sigma^2 2\pi^3 7\sigma^1 3\pi^1$ (0.645)
$A^2\Pi$	$5\sigma^2 6\sigma^2 2\pi^3 7\sigma^2 3\pi^0$ (0.918)		$5\sigma^2 6\sigma^2 2\pi^1 7\sigma^1 3\pi^3$ (0.099)		$5\sigma^2 6\sigma^1 2\pi^2 7\sigma^2 3\pi^2$ (0.088)
$1^4\Pi$	$5\sigma^2 6\sigma^2 2\pi^2 7\sigma^2 3\pi^1$ (0.916)		$5\sigma^2 6\sigma^1 2\pi^2 7\sigma^2 3\pi^2$ (0.085)		$5\sigma^2 6\sigma^2 2\pi^2 7\sigma^1 3\pi^2$ (0.082)
$1^4\Sigma^+$	$5\sigma^2 6\sigma^2 2\pi^3 7\sigma^1 3\pi^1$ (0.641)		$5\sigma^2 6\sigma^2 2\pi^2 7\sigma^1 3\pi^2$ (0.055)		$5\sigma^2 6\sigma^2 2\pi^1 7\sigma^1 3\pi^3$ (0.065)
	$5\sigma^2 6\sigma^2 2\pi^1 7\sigma^2 3\pi^3$ (0.147)	$2^4\Pi$	$5\sigma^2 6\sigma^1 2\pi^4 7\sigma^1 3\pi^1$ (0.856)		
	$5\sigma^2 6\sigma^1 2\pi^2 7\sigma^2 3\pi^2$ (0.098)	$1^6\Sigma^+$	$5\sigma^2 6\sigma^2 2\pi^2 7\sigma^1 3\pi^2$ (0.934)		

[a] Values in parentheses are the coefficients squared of configuration state function (CSF) associated with the electron configuration. Core configuration of each electronic state is $1\sigma^2 2\sigma^2 3\sigma^2 4\sigma^2 1\pi^4$.

Table 3
Spectroscopic parameters of eight electronic states for PN^+ calculated at the icMRCI + Q/56 + CV + DK level of theory.

State		D_e/cm^{-1}	T_e/cm^{-1}	R_e/Å	ω_e/cm^{-1}	$\omega_e\chi_e$/cm^{-1}	$10^2\omega_e y_e$/cm^{-1}	B_e/cm^{-1}	$10^3\alpha_e$/cm^{-1}
$X^2\Sigma^+$	This work	40,585.85	0.00	1.4817	1313.54	7.8619	4.207	0.79628	6.14
	Exp. [34]	40,577.36[a]	0.00	1.50±0.01	1306±3	7.9 ± 0.7			
	Exp. [39]		0.00	1.495	1303.9	7.62		0.781	1.5
	Cal. [38]	38,472.63	0.00	1.5150	1235.1			0.761	
	Cal. [42]	40,730.98	0.00	1.4789	1311.7	7.8063	4.0043	0.79918	6.106
$A^2\Pi$	This work	37,090.81	3493.48	1.5601	1148.09	7.0503	1.246	0.71821	5.78
	Exp. [37]	47,022.10	3387.53	1.565	1110				
	Cal. [38]	35,730.35	2742.28	1.565	1143.7			0.713	
	Cal. [42]	37,424.11	3384.7	1.5581	1146.4	6.9592	4.2173	0.72008	5.7658
$1^4\Sigma^+$	This work	16,319.30	24,266.41	1.6925	787.04	8.1752	12.54	0.61015	7.62
	Exp. [40]		(22,100±1600)[b]						
	Cal. [38]	15,889.12	22,583.51	1.7520	753.5			0.570	
	Cal. [42]	16,776.33	24,023.9	1.6863	799.8	4.8392	327.99	0.61383	4.425
$1^4\Pi$	This work	14,791.29	25,793.75	1.7956	710.66	4.9847	10.916	0.54283	6.08
	Exp. [40]		(22,100±1600)[b]						
	Cal. [38]	16,453.70	22,018.93	1.8140	787.3			0.513	
	Cal. [42]	15,243.87	25,547.1	1.7954	748.2	13.970	60.588	0.54257	5.8826
$1^4\Delta$	This work	17,716.96	31,230.27	1.6703	900.26	15.382	20.002	0.62926	7.47
	Cal. [38]	17,824.85	30,729.71	1.7290	952.9			0.585	
	Cal. [42]	18,308.78	30,714.4	1.6680	860.8	5.9874	8.0657	0.62817	6.346
$1^4\Sigma^-$	This work	12,824.45	36,118.26	1.6610	966.17	20.359	48.042	0.63847	7.12
	Cal. [38]	12,098.31	36,456.25	1.7350	849.3			0.58	
	Cal. [42]	12,985.52	35,621.8	1.6594	889.2	5.1991	22.284	0.63424	5.4997
$2^4\Pi$	This work	4052.49	62,969.21	1.4856	1219.03	6.5260	333.85	0.79026	5.58
	Cal. [42]	4436.05	61,393.9	1.4803	1245.7	20.010	212.32	0.79701	8.4701
$1^6\Sigma^+$	This work	6207.42	34,497.43	2.1594	364.63	3.9631	6.078	0.37570	5.63
	Cal. [42]	5807.19	35,018.5	2.1700	357.8	4.3749	0.64757	0.37135	5.6657

[a] Obtained by the D_0 value of Obase et al. [34] and the theoretical vibrational correction of this work.
[b] The possible experimental detection proposed by Reid [40].

$$\hat{g}_{s\alpha}(i,j) = \frac{1}{2c^2}\frac{\left[\mathbf{r}_{ij}\times\hat{\mathbf{p}}(i)\right]_\alpha}{r_{ij}^3} \tag{12}$$

where $\hat{g}_{s\alpha}(i,j)\cdot\hat{s}_\alpha(i)$ and $\hat{g}_{o\alpha}(i,j)\cdot\hat{s}_\alpha(i)$ are known as the spin-same-orbit and spin-other-orbit terms of the two-electron SO operator. All the symbols in Eqs. (5)–10 have their usual meanings which can be found in Ref. [58]. In icMRCI calculations, all configuration state functions of the CASSCF wave functions are used as a reference. Using these highly correlated wave functions, the SO coupling integrals between different electronic states of PN^+ are evaluated using the Breit-Pauli Hamiltonian as implemented in MOLPRO 2015 [54,55].

3. Results and discussions

3.1. Spectroscopic parameters and dipole moments

Fig. 1 provides an overview evolution of the PECs along the internuclear distance for the electronic states of PN^+ correlating to the two lowest dissociation asymptotes $P^+(^3P_g) + N(^4S_u)$ and $P^+(^1D_g) + N(^4S_u)$. These PECs are calculated at the icMRCI + Q/56 + CV + DK level of theory and are given in energy relative to the minimum of the ground state. As shown in Fig. 1, the $X^2\Sigma^+$, $A^2\Pi$, $1^4\Sigma^+$, $1^4\Pi$, $1^6\Sigma^+$, and $1^6\Pi$ states correspond to the lowest dissociation asymptote $P^+(^3P_g) + N(^4S_u)$. The $1^4\Sigma^-$, $2^4\Pi$, and $1^4\Delta$ states correlate to the second dissociation asymptote $P^+(^1D_g) + N(^4S_u)$. For the $2^4\Pi$ and $1^6\Pi$ states, apparent barriers occur around the internuclear distance of 1.7 Å, which are formed by avoiding crossing with the $3^4\Pi$ and $2^6\Pi$ states, respectively.

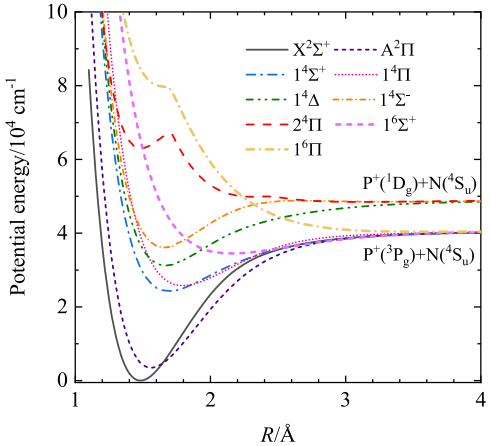

Fig. 1. The calculated icMRCI + Q/56 + CV + DK potential energy of nine electronic states of PN^+.

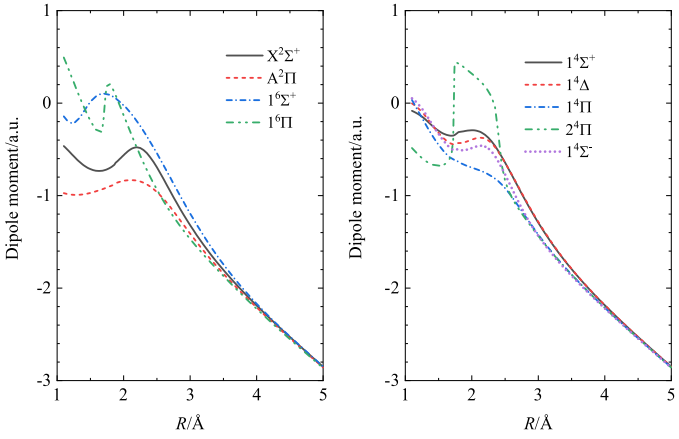

Fig. 2. Dipole moments for nine low-lying electronic states of PN^+.

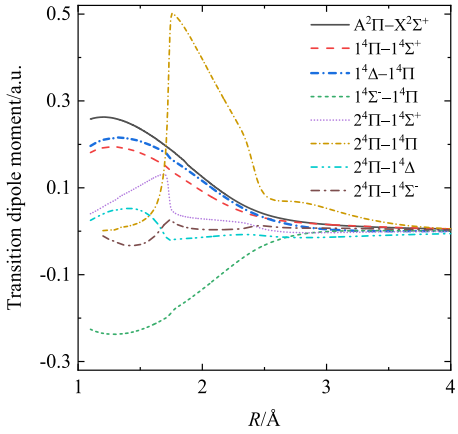

Fig. 3. TDMs of eight dipole allowed transitions between doublet or quartet states of PN^+. Note that the TDMs of the $1^4\Delta - 1^4\Pi$ and $2^4\Pi - 1^4\Delta$ systems are the Cartesian moment $\langle \Pi_x|y|\Delta_{xy}\rangle$, where $\langle \Pi \left|\frac{x+iy}{\sqrt{2}}\right|\Delta\rangle = \sqrt{2}\langle \Pi_x|y|\Delta_{xy}\rangle$.

Table 2 lists the leading electron configurations of eight bound and quasibound electronic states for PN^+ near their corresponding equilibrium internuclear distances. The calculated electron configuration of $PN(X^1\Sigma^+)$ state in our previous publication [32] is $5\sigma^2 6\sigma^2 2\pi^4 7\sigma^2 3\pi^0$ (0.899). The ground state $X^2\Sigma^+$ of PN^+ is mainly characterized by the $5\sigma^2 6\sigma^2 2\pi^4 7\sigma^1 3\pi^0$ (0.905) electronic configuration. Hence, the $PN^+(X^2\Sigma^+)$ is formed by loss of an electron from 7σ MO of PN $(X^1\Sigma^+)$ state. The $A^2\Pi$, $1^4\Sigma^+$, $1^4\Sigma^-$, $1^4\Delta$, and $2^4\Pi$ states of PN^+ are formed by single orbital excitation from its ground state, but the excited orbitals are different. For instance, the $A^2\Pi$ state is obtained after promotion of one electron from 2π MO to 7σ MO. For the $1^4\Sigma^+$,$1^4\Sigma^-$, and $1^4\Delta$ states, they have similar electron configurations and are all mainly described by the $2\pi^1 \rightarrow 3\pi^1$ electron excitation. It should be noted that the other electron configurations of the $1^4\Sigma^+$, $1^4\Sigma^-$, and

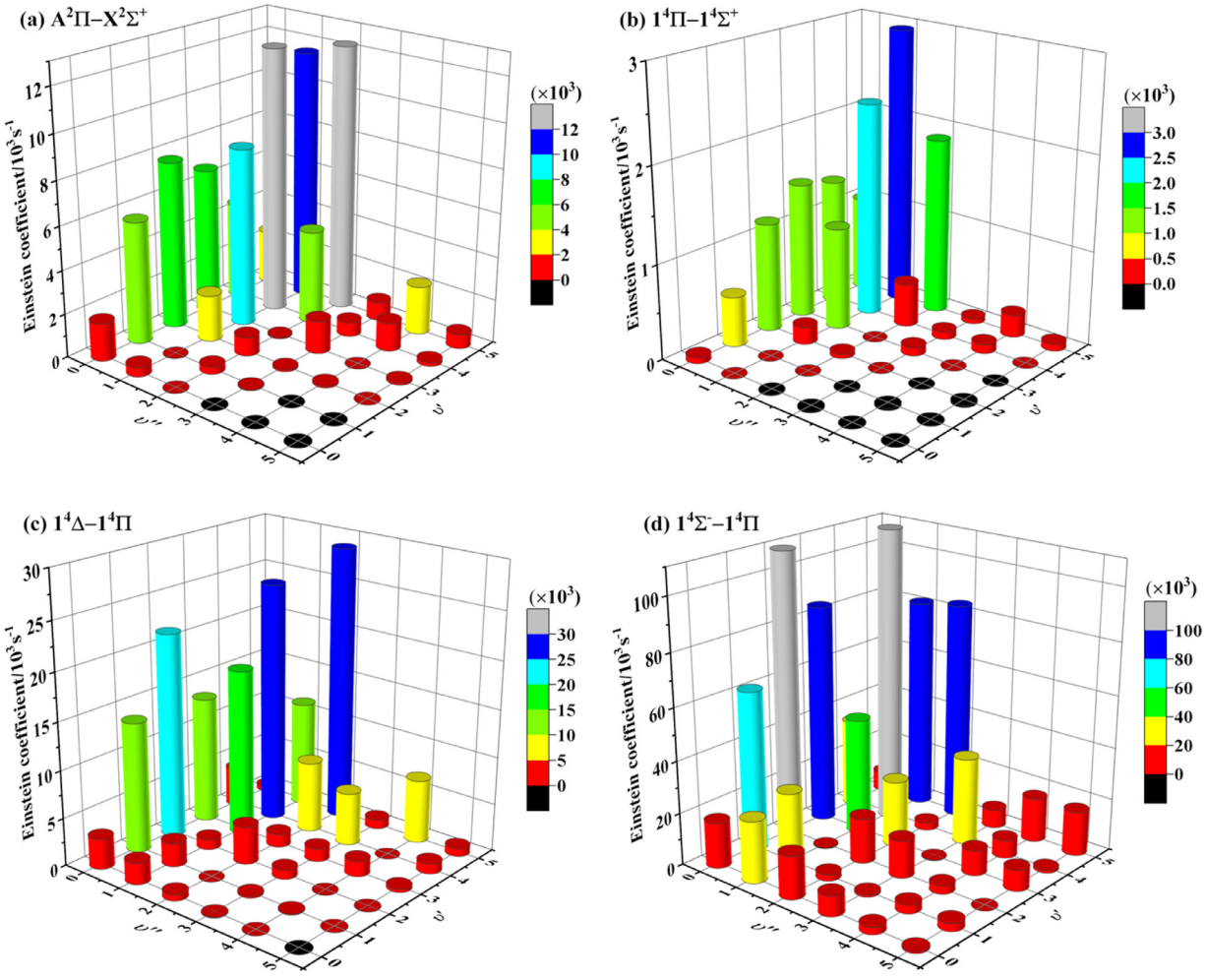

Fig. 4. Einstein coefficients of the (υ' = 0 – 5, υ" = 0 – 5) bands for the $A^2\Pi - X^2\Sigma^+$, $1^4\Pi - 1^4\Sigma^+$, $1^4\Delta - 1^4\Pi$, and $1^4\Sigma^- - 1^4\Pi$ systems of PN^+.

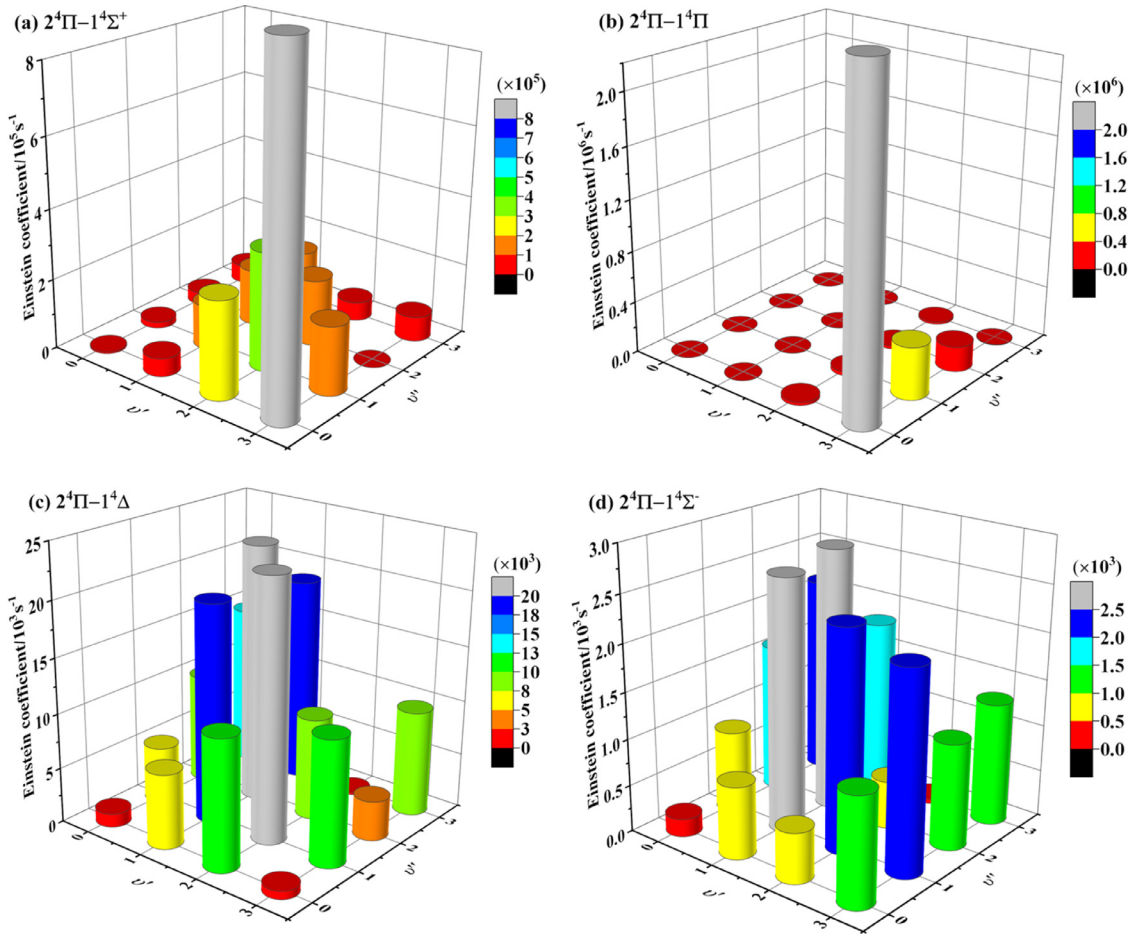

Fig. 5. Einstein coefficients of the (υ' = 0–3, υ" = 0 – 3) bands for the $2^4\Pi - 1^4\Sigma^+$, $2^4\Pi - 1^4\Pi$, $2^4\Pi - 1^4\Delta$, and $2^4\Pi - 1^4\Sigma^-$ systems of PN^+.

$1^4\Delta$ states are less important and their CSF-squared coefficients are lower than 0.15. The $2^4\Pi$ state corresponds to one electron excitation of 6σ MO into the vacant 3π MO. In addition, the $1^4\Pi$ and $1^6\Sigma^+$ states of PN^+ originate from the electronic configurations $5\sigma^2 6\sigma^1 2\pi^4 7\sigma^1 3\pi^1$ (0.856) and $5\sigma^2 6\sigma^2 2\pi^2 7\sigma^1 3\pi^2$ (0.934) corresponding to double electron promotions, i.e., $2\pi^2 \rightarrow 7\sigma^1 3\pi^1$ and $2\pi^2 \rightarrow 3\pi^2$, respectively.

Table 3 presents the spectroscopic parameters of eight bound and quasibound electronic states for PN^+. For the ground $X^2\Sigma^+$ state, its spectroscopic parameters are in good agreement with available experimental ones. The experimental D_0 deduced by Obase et al. [34] is 40,005.08 cm^{-1}. Combining with the theoretical vibrational correction of 572.28 cm^{-1} in this work, we calculate an experimental D_e value of 40,577.36 cm^{-1}. Our calculated D_e is only 8.49 cm^{-1} higher than this inferred one. The calculated ω_e, $\omega_e\chi_e$ and R_e are 1313.54 cm^{-1}, 7.8619 cm^{-1}, and 1.4817 Å, respectively, which agree well with the experimental values of 1306 cm^{-1}, 7.9 cm^{-1} and 1.50 Å [32] and the recent theoretical results [42] with very small deviations of 1.84 cm^{-1}, 0.0556 cm^{-1} and 0.0028 Å, respectively.

The calculated T_e and R_e of the $A^2\Pi$ state are 3493.48 cm^{-1} and 1.5601 Å, respectively, which are in good agreement with the only experimental values [37] of 3387.53 cm^{-1} and 1.565 Å, respectively. However, there are large deviations for ω_e and D_e between our computed ones and the experimental results, as shown in Table 3. It is worth noting that our computed ω_e and D_e agree well with the theoretical results [38,42]. Hence, new experiments are expected in the future to clarify such deviations.

For the quartet and sextet states, they lie at 24,000–63,000 cm^{-1} above the ground state. Experimentally, only Reid [40] suggested the possible detection of $1^4\Sigma^+$ and $1^4\Pi$ states at 22,100 ± 1600 cm^{-1}. Several theoretical work has been done to investigate their PECs and spectroscopic parameters. Our calculated spectroscopic parameters of them are in reasonable agreement with previous theoretical results [38,42]. However, dipole allowed transitions between the quartet or sextet states are not investigated before and will be presented in Section 3.2.

In order to clarify the polarity, bond nature, and relative stabilities of low-lying states for PN^+, dipole moment (DM) curves are calculated by the icMRCI approach with the AV6Z basis set and depicted in Fig. 2. With P at the origin and N along the positive direction of the internuclear axis, the DM curves are smooth along the internuclear distance for the $X^2\Sigma^+$, $A^2\Pi$, $1^4\Sigma^+$, $1^4\Pi$, $1^4\Delta$, $1^4\Sigma^-$, and $1^6\Sigma^+$ states, whereas the DM curves change sharply near the internuclear distance of 1.7 Å for the $2^4\Pi$ and $1^6\Pi$ states, corresponding to the barriers of the PECs of these two states (as shown in Fig. 1). It is not too surprising as the leading electron configurations of the $2^4\Pi$ and $1^6\Pi$ states are different for $R \leq 1.7$ Å and $R > 1.7$ Å, i.e., the leading electron configuration of the $2^4\Pi$ state changes from $5\sigma^2 6\sigma^1 2\pi^4 7\sigma^1 3\pi^1$ ($R \leq 1.7$ Å) to $5\sigma^2 6\sigma^2 2\pi^3 7\sigma^0 3\pi^2$ ($R > 1.7$ Å), and the leading electron configuration of the $1^6\Pi$ state changes from $5\sigma^2 6\sigma^2 2\pi^2 7\sigma^1 3\pi^1 8\sigma^1$ ($R \leq 1.7$ Å) to $5\sigma^2 6\sigma^1 2\pi^3 7\sigma^1 3\pi^2 8\sigma^0$ ($R > 1.7$ Å). The DM of each state tends to be a larger value at the dissociation limit, which means that the dissociation products of each state include the ionic fragment.

Table 4
Vibrational radiative lifetimes of the $A^2\Pi$ state via the $A^2\Pi - X^2\Sigma^+$ transition, of the $1^4\Pi$ state via the $1^4\Pi - 1^4\Sigma^+$ transition, of the $1^4\Delta$ state via the $1^4\Delta - 1^4\Pi$ transition, of the $1^4\Sigma^-$ state via the $1^4\Sigma^- - 1^4\Pi$ transition and of the $2^4\Pi$ state via the $2^4\Pi - 1^4\Sigma^+$, $2^4\Pi - 1^4\Pi$, $2^4\Pi - 1^4\Delta$ and $2^4\Pi - 1^4\Sigma^-$ transitions.

	$A^2\Pi$ - $X^2\Sigma^+$	$1^4\Pi - 1^4\Sigma^+$	$1^4\Delta - 1^4\Pi$	$1^4\Sigma^- - 1^4\Pi$	$2^4\Pi - 1^4\Sigma^+$	$2^4\Pi - 1^4\Pi$	$2^4\Pi - 1^4\Delta$	$2^4\Pi - 1^4\Sigma^-$
υ'	$\tau/\mu s$	τ/ms	$\tau/\mu s$	$\tau/\mu s$	$\tau/\mu s$	$\tau/\mu s$	$\tau/\mu s$	$\tau/\mu s$
0	462.3	28.68	183.6	14.49	1.822	78.37	8.656	75.06
1	166.4	19.99	71.42	9.931	1.168	30.53	8.248	80.88
2	92.00	0.737	42.47	6.830	0.856	6.492	8.605	99.38
3	60.03	0.386	32.24	5.642	0.654	0.312	12.20	99.23
4	42.94	0.236	24.21	4.699				
5	32.60	0.161	19.85	3.998				
6	25.82	0.119	16.46	3.483				
7	21.10	0.092	14.57	3.298				
8	17.69	0.073	13.59	3.060				
9	15.13	0.060	12.40	2.765				

3.2. Dipole allowed transition properties

TDMs of eight dipole allowed transitions of PN^+ are plotted in Fig. 3. The TDM curves of transitions from the $2^4\Pi$ state to the $1^4\Sigma^+$, $1^4\Pi$, $1^4\Delta$, and $1^4\Sigma^-$ states change abruptly around the internuclear distance of 1.7 Å, which is consistent with the sudden change of the leading electron configuration for the $2^4\Pi$ state near $R = 1.7$ Å, just as mentioned in Section 3.1.

Using ab initio PECs and TDMs, we compute the Einstein coefficients of these eight transition systems, as shown in Figs 4 and 5. The elaborate transition data of these systems, including Einstein coefficients and Franck-Condon factors, are tabulated in the supplemental material. Utilizing the Einstein coefficients, we determine the radiative lifetimes for several lower vibrational levels ($\upsilon' \leq 9$ if available) of the $A^2\Pi$, $1^4\Pi$, $1^4\Delta$, $1^4\Sigma^-$ and $2^4\Pi$ states, as summarized in Table 4. The $A^2\Pi$ state is the first excited state that has dipole allowed transitions, and it can decay radiatively to the ground state. Due to the relatively large TDMs for the transition from the $A^2\Pi$ state to the $X^2\Sigma^+$ state, there should be several strong emissions of the $A^2\Pi$ - $X^2\Sigma^+$ system. As shown in Fig. 4(a), the (1,0), (2,0), (3,0), (3,1), (4,1), (5,1), and (5,2) vibrational bands are all strong, and their Einstein coefficients are estimated to be 5.65×10^3, 7.73×10^3, 6.77×10^3, 8.26×10^3, 1.23×10^4, 1.16×10^4, and 1.23×10^4 s^{-1}, respectively. The calculated radiative lifetimes of the $A^2\Pi$ state are 462.3, 166.4, and 92.0 μs, respectively, for $\upsilon' = 0$, 1, 2. Unfortunately, no experimental data of this system are available in the literature. To help in possible observation of this system in the future, we calculate the vibrational band positions, which show that strong emissions lie in the infrared region.

As shown in Fig. 4(b), (c) and (d), strong emissions for the $1^4\Pi - 1^4\Sigma^+$, $1^4\Delta - 1^4\Pi$, and $1^4\Sigma^- - 1^4\Pi$ systems can be clearly observed according to the length of columns. The TDM curves of these three systems are similar along the internuclear distance. The values of TDM for these three systems are very close for any a given internuclear distance. Hence, intensities of emissions may be determined by the energy difference between the two electronic states of each system. Just as expected, the calculated Einstein coefficients for the $1^4\Sigma^- - 1^4\Pi$ system are the largest due to the largest energy difference between the $1^4\Sigma^-$ and $1^4\Pi$ states. The obtained Einstein coefficients for the $1^4\Pi - 1^4\Sigma^+$ system are the smallest.

As mentioned in Section 3.1, in order to avoid crossing with the $3^4\Pi$ state, a barrier emerges near $R = 1.7$ Å for the $2^4\Pi$ state, which forms a quite shallow potential well. It can only support four vibrational levels. The $2^4\Pi$ state has dipole allowed transitions to the lower $1^4\Sigma^+$, $1^4\Pi$, $1^4\Delta$, and $1^4\Sigma^-$ states. The calculated Einstein coefficients of the ($\upsilon' = 0 - 3$, $\upsilon'' = 0 - 3$) bands for these four systems are displayed in Fig. 5. Due to the larger energy separation between the $2^4\Pi$ and $1^4\Sigma^+$ states, Einstein coefficients of the $2^4\Pi - 1^4\Sigma^+$ system are larger than those of the other three systems for most vibrational bands, which means that the radiative lifetimes of the $2^4\Pi$ state are dominantly determined by decay to the $1^4\Sigma^+$ state. The vibrational radiative lifetimes of the $2^4\Pi$ state are about several microseconds. Such small radiative lifetimes mean that the $2^4\Pi$ state is hopefully to be observed by an approximate spectroscopic experiment.

Table 5
The definitions of the schematic expressions for SO couplings given in Fig. 6.

Expressions for SO coupling	Definitions
$X^2\Sigma^+ - A^2\Pi$	$<X^2\Sigma^+, m_s = -1/2\|L_xS_x\|A^2\Pi_y, m_s=1/2>$
$X^2\Sigma^+ - 1^4\Pi$	$<X^2\Sigma^+, m_s = 1/2\|L_xS_x\|1^4\Pi_y, m_s=3/2>$
$X^2\Sigma^+ - 2^4\Pi$	$<X^2\Sigma^+, m_s = 1/2\|L_xS_x\|2^4\Pi_y, m_s = 3/2>$
$X^2\Sigma^+ - 1^4\Sigma^-$	$<X^2\Sigma^+, m_s=1/2\|L_zS_z\|1^4\Sigma^-, m_s = 3/2>$
$A^2\Pi - 1^4\Sigma^+$	$<A^2\Pi_x, m_s = 1/2\|L_yS_y\|1^4\Sigma^+, m_s = 3/2>$
$A^2\Pi - 1^4\Pi$	$<A^2\Pi_x, m_s = 1/2\|L_zS_z\|1^4\Pi_y, m_s = 3/2>$
$A^2\Pi - 2^4\Pi$	$<A^2\Pi_x, m_s = 1/2\|L_zS_z\|2^4\Pi_y, m_s = 3/2>$
$A^2\Pi - 1^4\Sigma^-$	$<A^2\Pi_x, m_s = 1/2\|L_xS_x\|1^4\Sigma^-, m_s = 3/2>$
$A^2\Pi - 1^4\Delta$	$<A^2\Pi_x, m_s = 1/2\|L_yS_y\|1^4\Delta_x, m_s = 3/2>$
$1^4\Pi - 1^4\Sigma^+$	$<1^4\Pi_x, m_s = -3/2\|L_yS_y\|1^4\Sigma^+, m_s = 3/2>$
$1^4\Pi - 2^4\Pi$	$<1^4\Pi_x, m_s = 3/2\|L_zS_z\|2^4\Pi_y, m_s = 3/2>$
$1^4\Pi - 1^4\Sigma^-$	$<1^4\Pi_x, m_s = 3/2\|L_xS_x\|1^4\Sigma^-, m_s = 3/2>$
$1^4\Pi - 1^4\Delta$	$<1^4\Pi_x, m_s = 3/2\|L_yS_y\|1^4\Delta_x, m_s = 3/2>$
$1^4\Pi - 1^6\Sigma^+$	$<1^4\Pi_x, m_s = 3/2\|L_yS_y\|1^6\Sigma^+, m_s = 5/2>$
$1^4\Pi - 1^6\Pi$	$<1^4\Pi_x, m_s = 3/2\|L_zS_z\|1^6\Pi_y, m_s = 5/2>$
$2^4\Pi - 1^4\Sigma^+$	$<2^4\Pi_x, m_s = -3/2\|L_yS_y\|1^4\Sigma^+, m_s = 3/2>$
$2^4\Pi - 1^4\Delta$	$<2^4\Pi_x, m_s = 3/2\|L_yS_y\|1^4\Delta_x, m_s = 3/2>$
$2^4\Pi - 1^4\Sigma^-$	$<2^4\Pi_x, m_s = 3/2\|L_xS_x\|1^4\Sigma^-, m_s = 3/2>$
$2^4\Pi - 1^6\Sigma^+$	$<2^4\Pi_x, m_s = 3/2\|L_yS_y\|1^6\Sigma^+, m_s = 5/2>$
$2^4\Pi - 1^6\Pi$	$<2^4\Pi_x, m_s = 3/2\|L_zS_z\|1^6\Pi_y, m_s = 5/2>$
$1^4\Sigma^+ - 1^4\Sigma^-$	$<1^4\Sigma^+, m_s = 3/2\|L_zS_z\|1^4\Sigma^-, m_s = 3/2>$
$1^4\Sigma^+ - 1^6\Pi$	$<1^4\Sigma^+, m_s = 3/2\|L_xS_x\|1^6\Pi_y, m_s = 5/2>$
$1^4\Delta - 1^6\Pi$	$<1^4\Delta_x, m_s = 3/2\|L_yS_y\|1^6\Pi_x, m_s = 5/2>$
$1^4\Sigma^- - 1^6\Sigma^+$	$<1^4\Sigma^-, m_s = 3/2\|L_zS_z\|1^6\Sigma^+, m_s = 5/2>$
$1^4\Sigma^- - 1^6\Pi$	$<1^4\Sigma^-, m_s = 3/2\|L_xS_x\|1^6\Pi_x, m_s = 5/2>$
$1^6\Sigma^+ - 1^6\Pi$	$<1^6\Sigma^+, m_s=-5/2\|L_xS_x\|1^6\Pi_y, m_s = 5/2>$

3.3. Spin-orbit coupling and predissociation

Fig. 6 displays the evolution of the SO coupling integrals related to low-lying electronic states of PN^+ along the internuclear distance. These integrals are computed at the CASSCF/MRCI/AV6Z level of theory. The definitions of the schematic expressions for SO couplings given in Fig. 6 are listed in Table 5. As shown in Fig. 6(a), the values of SO coupling integrals $X^2\Sigma^+ - A^2\Pi$, $X^2\Sigma^+ - 1^4\Pi$, $X^2\Sigma^+ - 2^4\Pi$, and $X^2\Sigma^+ - 1^4\Sigma^-$ are larger than 30 cm^{-1} at large internuclear distances, which means that the splitting of the $X^2\Sigma^+$ state at the dissociation limit is affected by all the adjacent states within the selection rules of SO couplings. In

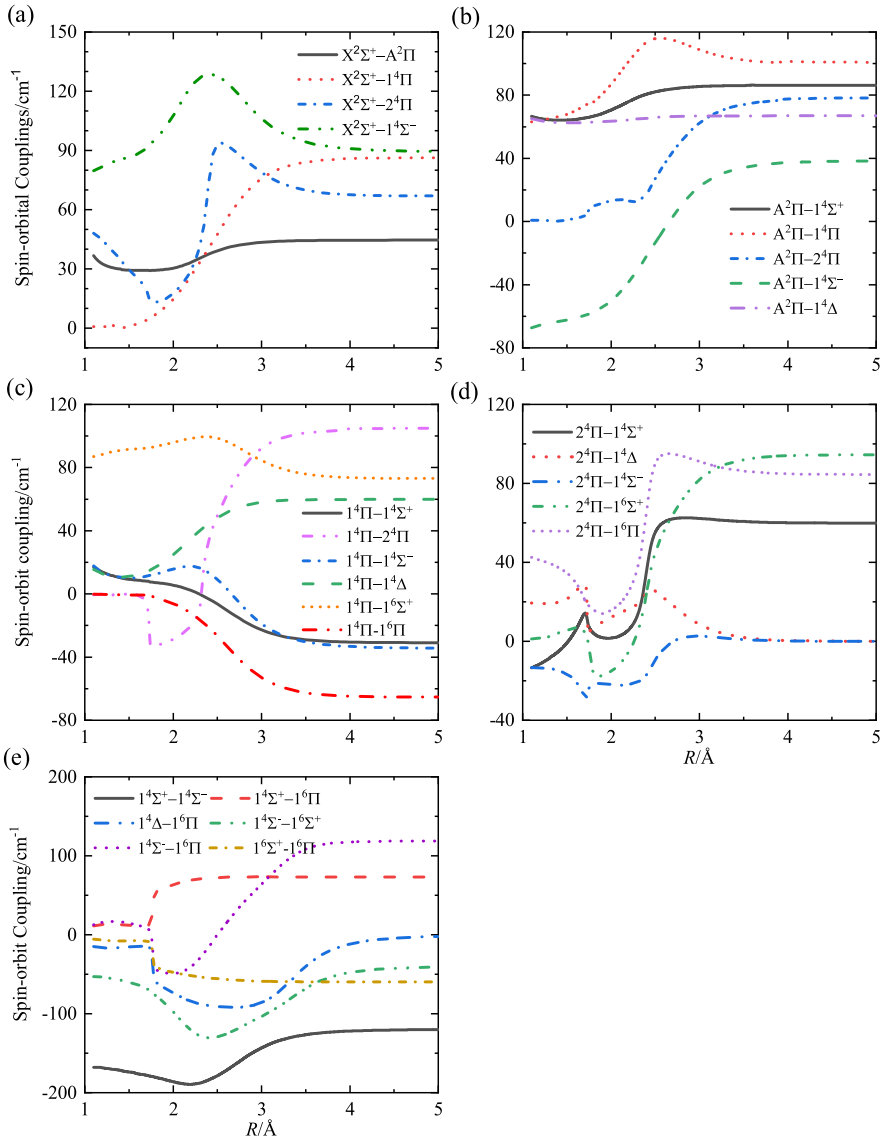

Fig. 6. Evolution of spin-orbit couplings related to low-lying electronic states of PN^+.

the Franck-Condon region, the values of the SO coupling integrals $X^2\Sigma^+ - A^2\Pi$ and $X^2\Sigma^+ - 1^4\Sigma^-$ are in the range of 30–130 cm^{-1}, which are large enough to influence the electronic structure of the $X^2\Sigma^+$ state by SO coupling. Fig. 6(b) shows that the absolute values of SO coupling integrals $A^2\Pi - 1^4\Sigma^-$, $A^2\Pi - 1^4\Sigma^+$, $A^2\Pi - 1^4\Pi$, $A^2\Pi - 2^4\Pi$, $A^2\Pi - 1^4\Delta$ are larger than 40 cm^{-1} at the dissociation limit, so the SO couplings between the $A^2\Pi$ state and the $1^4\Sigma^-$, $1^4\Sigma^+$, $1^4\Pi$, $2^4\Pi$, as well as $1^4\Delta$ states impact the splitting of the $A^2\Pi$ state at large internuclear distances. Similar analyzation can be applied to other electronic states according to the given SO coupling integrals in Fig. 6(c), (d), and (e). Due to the change in the dominant electron configurations of the $2^4\Pi$ and $1^6\Pi$ states around $R = 1.7$ Å, the SO coupling integrals related to these two states change drastically between $R \leq 1.7$ Å and $R > 1.7$ Å.

As shown in Fig. 1, there is an intersection between the $X^2\Sigma^+$ and $A^2\Pi$ states around $R = 1.65$ Å, lying in the vibrational levels $\upsilon' = 3$ and 4 of the $X^2\Sigma^+$ state. Fig. 6(a) exhibits that the SO coupling integral $X^2\Sigma^+ - A^2\Pi$ is 29.35 cm^{-1} at $R = 1.65$ Å, which is large enough to allow SO conversion. For the $1^4\Pi$ state, this situation is rather complicated since the $1^4\Pi$ state is embedded into a set of PECs of electronic states to which it can couple. Specifically, the $1^4\Pi$ state is crossed by the $1^4\Sigma^-$, $1^4\Delta$, $1^4\Sigma^+$, and $1^6\Sigma^+$ states. The $1^4\Pi - 1^4\Sigma^-$, $1^4\Pi - 1^4\Delta$, $1^4\Pi - 1^4\Sigma^+$, and $1^4\Pi - 1^6\Sigma^+$ SO conversions are all allowed. The values of SO coupling integrals $1^4\Pi - 1^4\Sigma^-$, $1^4\Pi - 1^4\Delta$, $1^4\Pi - 1^4\Sigma^+$, and $1^4\Pi - 1^6\Sigma^+$ are calculated to be 10.29, 11.41, 6.81, 99.32 cm^{-1} at their respective crossings (i.e., $R = 1.43$ Å, $R = 1.54$ Å, $R = 1.86$ Å, and $R = 2.42$ Å) allowing such SO conversions.

The $1^4\Sigma^-$ and $1^4\Delta$ states are crossed by the $1^6\Sigma^+$ and $1^6\Pi$ states. For the $1^4\Sigma^-$ state, the two crossings reside in the vibrational levels $\upsilon' = 1$ and $\upsilon' = 15$ of the $1^4\Sigma^-$ state. The calculated SO coupling integrals are −76.82 and −28.42 cm^{-1} at their corresponding crossings, which can provide a strong predissociation pathway of $1^4\Sigma^-$ ($\upsilon' = 1$)→$1^6\Sigma^+$ and $1^4\Sigma^-$ ($\upsilon' = 15$)→$1^6\Pi$, respectively. Although the $1^4\Delta$ state is also crossed by the $1^6\Sigma^+$ and $1^6\Pi$ states, only the $1^4\Delta - 1^6\Pi$ SO coupling is allowed. Because of the large value of −90.93 cm^{-1} for the SO coupling integral $1^4\Delta - 1^6\Pi$ at the crossing $R = 2.52$ Å, there should be a strong predissociation pathway of $1^4\Delta$ ($\upsilon' = 19$)→$1^6\Pi$.

4. Conclusions

In this work, the icMRCI + Q/56 + CV + DK method is used to calculate the PECs of nine electronic states correlated with the two lowest dissociation asymptotes $P^+(^3P_g)$ + $N(^4S_u)$ and $P^+(^1D_g)$ + $N(^4S_u)$. TDMs of dipole allowed transitions have been computed at the icMRCI/AV6Z level of theory. Based on the calculated PECs, we determine the spectroscopic parameters for eight bound and quasi-bound states, which agree well with available experimental and theoretical results. PECs and TDMs are used to calculate the transition probabilities of dipole allowed transition systems. The vibrational radiative lifetimes of some excited states are also evaluated. The obtained transition data can provide guidelines for experimental observations. By analyzation of the SO couplings, the SO coupling integral $X^2\Sigma^+ - A^2\Pi$ is 29.35 cm^{-1} at $R = 1.65$ Å, which is large enough to allow SO conversion. The values of SO coupling integrals $1^4\Pi - 1^4\Sigma^-$, $1^4\Pi - 1^4\Delta$, $1^4\Pi - 1^4\Sigma^+$, and $1^4\Pi - 1^6\Sigma^+$ are calculated to be 10.29, 11.41, 6.81, 99.32 cm^{-1} at their respective crossings, also allowing such SO conversions. Moreover, the absolute values of SO coupling integrals $1^4\Sigma^- - 1^6\Sigma^+$, $1^4\Sigma^- - 1^6\Pi$, and $1^4\Delta - 1^6\Pi$ are 76.82, 28.42, and 90.93 cm^{-1} at their respective crossings, which can provide strong predissociation pathways of $1^4\Sigma^-$ ($\upsilon' = 1$)→$1^6\Sigma^+$, $1^4\Sigma^-$ ($\upsilon' = 15$)→$1^6\Pi$ and $1^4\Delta$ ($\upsilon' = 19$)→$1^6\Pi$.

Acknowledgements

This work is sponsored by the National Natural Science Foundation of China under Grant no. 51336002, 51421063.

Supplementary materials

Supplementary material associated with this article can be found, in the online version, at doi:10.1016/j.jqsrt.2019.05.024.

References

[1] Turner BE, Bally J. Detection of interstellar PN: the first identified phosphorus compound in the interstellar medium. Astrophys J 1987;321:L75–LL9.
[2] Ziurys LM. Detection of interstellar PN: the first phosphorus-bearing species observed in molecular clouds. Astrophys J 1987;321:L81.
[3] Turner BE, Tsuji T, Bally J, Guelin M, Cernicharo J. Phosphorus in the dense interstellar medium. Astrophys J 1990;365:569–85.
[4] Milam SN, Halfen DT, Tenenbaum ED, Apponi AJ, Woolf NJ, Ziurys LM. Constraining phosphorus chemistry in carbon- and oxygen-rich circumstellar envelopes: observations of PN, HCP, and CP. Astrophys J 2008;684:618–25.
[5] Yamaguchi T, Takano S, Sakai N, Sakai T, Liu S-Y, Su Y-N, Hirano N, Takakuwa S, Aikawa Y, Nomura H. Detection of phosphorus nitride in the lynds 1157 B1 shocked region. Pub Astron Soc Jap 2011;63:L37–41.
[6] Beck ED, Kamiński T, Patel NA, Young KH, Gottlieb CA, Menten KM, Decin L. PO and PN in the wind of the oxygen-rich AGB star IK Tau. Astron Astrophys 2013;558:132–40.
[7] Fontani F, Rivilla VM, Caselli P, Vasyunin A, Palau A. Phosphorus-bearing molecules in massive dense cores. Astrophys J 2016;822:30.
[8] Lefloch B, Vastel C, Viti S, Jimenezserra I, Codella C, Podio L, Ceccarelli C, Mendoza E, Lepine JRD, Bachiller R. Phosphorus-bearing molecules in solar-type star-forming regions: first PO detection. Mon Not R Astron Soc 2016;462:3937–44.
[9] Rivilla VM, Fontani F, Beltrán MT, Vasyunin A, Caselli P, MartínPintado J, Cesaroni R. The first detections of the key prebiotic molecule PO in star-forming regions. Astrophys J 2016;826:161.
[10] Rivilla VM, Jiménezserra I, Zeng S, Martín S, Martínpintado J, Armijosabendaño J, Viti S, Aladro R, Riquelme D, Requenatorres M. Phosphorus-bearing molecules in the Galactic Center. Mon Not R Astron Soc 2018:475.
[11] Ziurys LM, Schmidt DR, Bernal JJ. New circumstellar sources of PO and PN: the increasing role of phosphorus chemistry in oxygen-rich stars. Astrophys J 2018;856:169.
[12] Curry J, Herzberg L, Herzberg G. Spektroskopischer Nachweis und Struktur des PN-Moleküls. Zeitschrift Für Physik 1933;86:348–66.
[13] Curry J, Herzberg L, Herzberg G. Spectroscopic evidence for the molecule PN. J Chem Phys 1933;1:749.
[14] Ghosh PN, Datta AC. Das Bandenspektrum des Phosphornitrids. Zeitschrift Für Physik 1934;87:500–4.
[15] Raymonda J, Klemperer W. Molecular beam electric resonance spectrum of $^{31}P^{14}N$. J Chem Phys 1971;55:232–3.
[16] Wyse FC, Manson EL, Gordy W. Millimeter wave rotational spectrum and molecular constants of $^{31}P^{14}N$. J Chem Phys 1972;57:1106–8.
[17] Moeller MB, Silvers SJ. Fluorescence spectra of PN and BF☆. Chem Phys Lett 1973;19:78–81.
[18] Moeller MB, Mckeever MR, Silvers SJ. Hanle effect measurement of the lifetime of the $A^1\Pi$ state of PN. Chem Phys Lett 1975;31:398–400.
[19] Gottscho RA, Field RW, Lefebvre-Brion H. Ab initio and semiempirical estimates of PN valence state interactions. J Mol Spectrosc 1978;70:420–31.
[20] Coquart B, Prudhomme JC. A new electronic transition of the PN molecule. J Phys B-At Mol Opt Phys 1980;13:2251–4.
[21] Coquart B, Prudhomme JC. The $^1\Sigma^+$-$X^1\Sigma^+$ transition of the PN molecule. J Mol Spectrosc 1981;87:75–84.
[22] Ghosh SN, Verma RD, Vanderlinde J. A high resolution study of $A^1\Pi$-$X^1\Sigma$ transition of the PN molecule. Can J Phys 1981;59:1640–52.
[23] Grein F, Kapur A. The electronic spectrum of PN. A configuration interaction study. J Mol Spectrosc 1983;99:25–34.
[24] Saraswathy P, Krishnamurty G. Isotope shifts in theA 1 Π− X 1 Σ+ system of PN molecule. Pramana 1984;23:665–9.
[25] Saraswathy P, Krishnamurty G. Rotational analysis of $A^1\Pi$-$X^1\Sigma^+$ bands of $P^{14}N$ and $P^{15}N$: perturbatio studies in the $A^1\Pi$ state. Pramana 1987;29:53–77.
[26] Bredohl H, Dubois I, Macau-Hercot D, Remy F, Breton J, Esteva JM. Rydberg states of PN. J Mol Spectrosc 1992;156:292–5.
[27] Ahmad IK, Hamilton PA. The Fourier transform infrared spectrum of PN. J Mol Spectrosc 1995;169:286–91.
[28] Floch ACL, Melen F, Dubois I, Bredohl H. A new study of the perturbations in the $A^1\Pi$ State of PN. J Mol Spectrosc 1996;176:75–84.
[29] Cazzoli G, Cludi L, Puzzarini C. Microwave spectrum of $P^{14}N$ and $P^{15}N$: spectroscopic constants and molecular structure. J Mol Struct 2006;780:260–7.
[30] Wang J, Sun J, Shi D. Accurate ab initio study of low-lying electronic states of phosphorus nitride radical. Chin Phys B 2010;19:340–6.
[31] Abbiche K, Salah M, Marakchi K, Kabbaj OK, Komiha N. Ab initio study of PN electronic states: a qualitative interpretation of the perturbation and predissociation effects on observed transitions. Mol Phys 2014;112:117–26.
[32] Qin Z, Zhao J, Liu L. Energy levels, transition dipole moment, transition probabilities and radiative lifetimes for low-lying electronic states of PN. J Quant Spectrosc Radiat Transf 2019;227:47–56.
[33] Obase H, Tsuji M, Nishimura Y. PN^+ ($B^2\Sigma^+$-$X^2\Sigma^+$) emission produced from penning ionizatton of transient PN ($X^1\Sigma^+$) radicals. Chem Phys Lett 1981;81:119–22.
[34] Obase H, Tsuji M, Nishimura Y. Energy-transfer reactions between He (2^3S) and Ne ($^3P_{0,2}$) metastable atoms and PN radicals. Chem Phys 1983;74:89–95.
[35] Obase H, Tsuji M, Nishimura Y. Emission spectra produced from thermal energy charge transfer reactions of Ar^+ ions with CS and PN radicals. Chem Phys 1984;87:93–9.
[36] Imajo T, Tokieda K, Nakashima Y, Tanaka K, Tanaka T. High-resolution Fourier transform emission spectroscopy of the $B^2\Sigma^+(v=0)$-$X^2\Sigma^+(v=0)$ transition of the PN^+ Ion. J Mol Spectrosc 2000;204:21.
[37] Bulgin DK, Dyke JM, Morris A. Vacuum ultraviolet photoelectron spectrum of the PN ($X^1\Sigma^+$) molecule. J Chem Soc Faraday Transac 2 1977;73:983–90.
[38] Grein F. Electronic states of PN^+ obtained by configuration-interaction studies. Chem Phys 1988;120:383–8.
[39] Ahmad IK, Hamilton PA. A High-resolution study of the $B^2\Sigma^+$-$X^2\Sigma^+$ transition of the PN^+ molecular ion. J Mol Spectrosc 1994;163:214–20.
[40] Reid C. Energies of the lowest quartet states in PN^+ and P_2^+, determined using charge-inversion spectroscopy. Chem Phys Lett 1994;229:279–84.
[41] Bruna PJ, Grein F. Theoretical study on N_2^+, P_2^+, As_2^+, NP^+, NAs^+, and PAs^+: hyperfine coupling constants for $1^2\Sigma_g^+$, and electron-spin g-factors for $1^2\Sigma_g^+/1$, $2^2\Sigma_u^+$ (X_2^+) and 1, $2^2\Sigma^+$(XY^+) states. J Mol Spectrosc 2005;232:137–50.
[42] Zhu Z, Zhou D, Wang X, Shi D, Sun J. These effects of spin-orbit coupling, core–valence correlation and scalar relativistic correction on spectroscopic calculations for PN^+ cation. Comput Theor Chem 2016;1079:23–33.
[43] Malicet J, Brion J, Guenebaut H. Spectre du radical P_2^+: etude des transitions $C^2\Pi$-$X^2\Pi$ et $D^2\Pi$-$X^2\Pi$. Can J Phys 1976;54:907–14.
[44] Collet D, Destombes J-L, Bachir IH, Huet T. Rotational analysis of the vibrational hot bands of N_2^+ ($A^2\Pi_u$-$X^2\Sigma_g^+$) in the near-infrared region using velocity modulation spectroscopy. Chem Phys Lett 1998;286:311–16.
[45] Bruna PJ, Grein F. The A2Πu state of N2+: electric properties, fine and hyperfine coupling constants, and magnetic moments (g-factors). A theoretical study. J Mol Spectrosc 2008;250:75–85.
[46] NIST. https://physics.nist.gov/PhysRefData/ASD/levels_form.html.
[47] Knowles PJ, Werner HJ. An efficient second-order MCSCF method for long configuration expansions. Chem Phys Lett 1985;115:259–67.
[48] Knowles PJ, Werner HJ. An efficient method for the evaluation of coupling coefficients in configuration interaction calculations. Chem Phys Lett 1988;145:514–22.
[49] Werner HJ, Knowles PJ. An efficient internally contracted multiconfiguration reference CI method. J Chem Phys 1988;89:5803–14.
[50] Woon DE, Dunning Jr TH. Gaussian basis sets for use in correlated molecular calculations. V. Core-valence basis sets for boron through neon. J Chem Phys 1995;103:4572–85.
[51] de Jong WA, Harrison RJ, Dixon DA. Parallel Douglas-Kroll energy and gradients in NWChem: estimating scalar relativistic effects using Douglas-Kroll contracted basis sets. J Chem Phys 2001;114:48–53 .
[52] Truhlar DG. Basis-set extrapolation. Chem Phys Lett 1998;294:45–8.
[53] Fast PL, Sánchez MAL, Truhlar DG. Infinite basis limits in electronic structure theory. J Chem Phys 1999;111:2921–6.

[54] Werner H-J, Knowles PJ, Knizia G, Manby FR, Schütz M. WIREs Comput Mol Sci 2012;2:242–53.
[55] Werner H.-J., Knowles P.J., Knizia G., Manby F.R., others a. MOLPRO, a package of ab initio programs, see http://www.molpronet 2015.
[56] Laux CO, Kruger CH. Arrays of radiative transition probabilities for the N_2 first and second positive, NO β and γ, N_2^+ first negative, and O_2 Schumann-Runge band systems. J Quant Spectrosc Radiat Transf 1992;48:9–24.
[57] da Silva ML, Dudeck M. Arrays of radiative transition probabilities for CO_2–N_2 plasmas. J Quant Spectrosc Radiat Transf 2006;102:348–86.
[58] Berning A, Schweuzer M, Werner H-J, Knowles P, Palmieri P. Spin-orbit matrix elements for internally contracted multireference configuration interaction wavefunctions. Mol Phys 2000;98:1823–33.